BNL-95332-2011-JA

SENSITIVITY OF IDEALIZED SQUALL LINE SIMULATIONS TO THE LEVEL OF COMPLEXITY USED IN TWO TWO-MOMENT BULK MICROPHYSICS SCHEMES

Kwinten Van Weverberg[1], Andrew M. Vogelmann[1], Hugh Morrison[2], Jason Milbrandt[3]

[1]*Brookhaven National Laboratory, Upton, NY, USA*
[2]*National Center for Atmospheric Research, Boulder, CO, USA*
[3]Numerical Weather Prediction Section, Meteorological Research Division, Environment Canada, Dorval, QB, Canada.

Submitted to the
Monthly Weather Rev.

June 2011

Atmospheric Sciences Division/Environmental Sciences Dept.

Brookhaven National Laboratory

U.S. Department of Energy
Office of Science

DISCLAIMER

Abstract

In this paper the level of complexity that is needed within bulk microphysics schemes to represent the essential features associated with deep convection is investigated. To do so, the sensitivity of surface precipitation is evaluated in two-dimensional idealized squall line simulations to the level of complexity in the bulk microphysics schemes of Morrison et al. (2009) and the Milbrandt and Yau (2005). Factors examined include the number of predicted moments for each of the precipitating hydrometeors, the number and nature of ice categories, and several conversion term formulations. First, it was shown that the explicit prediction of mixing ratio and number concentration (i.e., fully two-moments) of *all* precipitating hydrometeors was required to represent size sorting, which significantly impacted peak precipitation. In addition, cold pools weakened when rain and graupel number concentrations were explicitly predicted, since size sorting led to larger graupel particles that melted into larger rain drops and caused less evaporative cooling. Second, surface precipitation was found to be less sensitive to the nature of the rimed ice species (hail or graupel). Including both hail and graupel led to a decrease of peak precipitation; however, it was also found that the production of hail strongly depends on an unphysical threshold that converts small hail back to graupel, which indicates the need for a more physical treatment of the graupel-to-hail conversion. Third, it was shown that the differences in precipitation extremes between the two two-moment microphysics schemes are mainly related to the treatment of collisional drop breakup. It was also shown that while the Morrison et al. (2009) scheme is dominated by deposition growth and low precipitation efficiency, the Milbrandt and Yau (2005) scheme is dominated by riming processes and high precipitation efficiency. More generally, this research suggests that improved formulations of collection and deposition, based laboratory experiments and field campaigns should be one of the primary foci for model improvement over the next years.

Introduction

A proper representation of deep convection is of primary importance to climate models and numerical weather prediction (NWP) models, as the latent heat associated with it drives atmospheric circulations. It is also associated with the most intense precipitation events occurring in the midlatitudes and the tropics. Many NWP models now operate at convection permitting horizontal grid spacing of only a few km, at which convection parameterizations are typically not used. This has brought the role of microphysics in the simulation of deep convection in the middle of the research spotlight over recent years (e.g., McCumber et al. 1991, Gilmore et al. 2004, Dawson et al. 2010, Morrison and Milbrandt 2011).

Bulk microphysics schemes are the workhorses in both NWP and climate modeling and typically apply conversion formulations to one or more bulk quantities of the particle size distribution of a number of hydrometeors. A variety of such bulk microphysics parameterizations have been developed over the past decades, with gradually increasing complexity. The most basic of those schemes predict only the mixing ratio of a few hydrometeor types ('one-moment schemes'). Typically, such models contain precipitating and non-precipitating liquid (Kessler 1969) and ice water (Cotton 1982). Later, complexity was added to those models by adding different ice categories, such as graupel (Rutledge and Hobbs 1983), hail (Lin et al. 1983), and even adding up to ten ice categories (Straka and Mansell 2005). Other models tend to have more complexity by not only predicting the mixing ratio, but also the number concentration of the hydrometeors ('two-moment schemes', e.g., Morrison et al. 2009, Seifert and Beheng 2001) and the radar reflectivity ('three-moment schemes', e.g., Milbrandt and Yau 2005). Most complex schemes have left the 'bulk' assumption of the different predicted water species and apply microphysical formulations to several separate size distribution bins ('spectral schemes', e.g., Kogan 1991, Khain et al. 1999). However, since these spectral models are much more

computationally expensive than bulk schemes, they are not yet used operationally. While bulk microphysics schemes with prognostic hydrometeors were developed mainly for NWP, they are now being more commonly used in climate models, particularly as enhanced computational resources enable climate models to operate at horizontal grid spacings comparable to those in NWP.

Given the computational burden these complex bulk parameterizations impose on NWP and climate simulations, a critical question to be answered is what level of complexity is needed to represent the essential features associated with deep convection. A number of publications suggested adding complexity to existing bulk microphysics schemes by increasing the number of ice categories for the simulation of convective and stratiform precipitation (McCumber et al. 1991, Ferrier et al. 1995, Van Weverberg et al. 2011a). They showed that this increased the overall realism of their simulations. Further, two-moment schemes have been shown to better capture the structure of supercells (Dawson et al. 2010) and squall lines (Morrison et al. 2009) than one-moment schemes and the simulation of orographic precipitation has been shown to be sensitive to the number of prognostic moments (Milbrandt et al. 2010). Triple-moment schemes were mostly similar to two-moment schemes (Dawson et al. 2010, Milbrandt et al. 2010). It remains debatable, however, whether the increased computing power should be primarily used to increase the number of hydrometeor classes or the number of predicted moments. Similarly, while most of the previous work confronted fully one-moment and fully two-moment schemes, there is little published work on the impact of separately predicting more moments of each hydrometeor class.

Another outstanding issue regarding complex microphysics parameterizations is the reason for the considerable variation in the behavior of similarly complex models (e.g., Morrison and Milbrandt 2011). As long as it is unknown why these models differ in terms of surface

precipitation and the representation of moist convection, it will remain a challenge to learn from model-observation comparisons and bring forward ways for model improvement.

To address these issues, this paper describes a number of sensitivity experiments imposed on a 2D-squall line simulation within the context of two commonly used two-moment microphysics schemes (Morrison et al. 2009 and Milbrandt and Yau 2005). First, we examined the role of the number of predicted moments for each precipitating hydrometeor class separately by changing fully one-moment versions of the aforementioned schemes step by step (hydrometeor class by hydrometeor class) back to the fully two-moment schemes. Second, we increased the number of precipitating ice categories by extending versions of both schemes, which contain only snow and graupel as precipitating ice categories, to also include hail. A last set of experiments was designed to understand why similar versions of both schemes still yield considerable differences in terms of surface precipitation and moist processes aloft. To that end, we systematically replaced parts of one microphysics scheme by the formulations of the other scheme until both schemes became identical.

The next section discusses the model setup applied in all these experiments, which are themselves explained in detail in section 2.2. Results are documented in section 3 and discussed and summarized in section 4.

1. Model description and experimental design

1.1 Model description

The Advanced Research Weather Research and Forecasting model (ARW-WRF) Version 3.2 (Skamarock et al. 2007) was used for all experiments in this study, applying the standard 2-D idealized squall line case available within the WRF package. Initialization of the model was done using the environmental sounding of Weisman and Klemp (1984), which represents a

midlatitude continental squall line environment. The 2-D framework allows for a large number of experiments, yet still captures the essential structure perpendicular to the line of propagation. The domain consisted of a 600 km × 20 km vertical cross section with a horizontal grid spacing of 1 km and a vertical grid spacing of 250 m. Turbulence was represented by a 1.5-order turbulent kinetic energy (TKE) scheme, while radiation and boundary layer processes were turned off. All simulations were integrated over 5 hours.

Microphysical processes are represented by either the Morrison et al. (2009, hereafter MTT) or the Milbrandt and Yau (2005, hereafter MY) two-moment schemes. Both schemes were modified from the original version in WRF Version 3.2 in order to make them as identical in setup as possible. Both schemes include two-moment cloud water and ice and have three precipitating hydrometeor classes: rain, snow and graupel. Relevant prescribed size distribution and fall speed parameters are listed in Table 1, which are identical for both schemes in this study. Size distributions of all precipitating hydrometeors in both schemes are represented by negative exponential functions of the form:

$$N_x(D) = N_{0x} e^{-\lambda_x D} \qquad (1)$$

where N_{0x} and λ_x are the intercept and slope parameters respectively, and D is the particle diameter. The parameter can be calculated from the mixing ratio (q_x, in kg kg^{-1}) and number concentration (N_x, in kg^{-1}) by:

$$\lambda_x = \left[\frac{a_{mx} N_x \Gamma(b_{mx} + 1)}{q_x} \right]^{1/(b_{mx})} \qquad (2)$$

where a_{mx} and b_{mx} are the parameters of the mass-diameter power-law relation, listed in Table 1. In these schemes, all hydrometeors are assumed to be spherical. Mass and number-concentration-

weighted bulk fall velocities for all hydrometeor species are calculated based on empirical power-law velocity-diameter relationships:

$$V_x(D) = a_{vx} D^{b_{vx}} \qquad (3)$$

where a_{vx} and b_{vx} are empirically derived parameters, listed in Table 1.

In order to make a close comparison between both schemes, continental aerosol concentrations were prescribed in both schemes, where these concentrations followed a lognormal distribution in the MTT and a polynomial distribution in MY. This leads to lower aerosol concentrations in MY, mainly at lower altitudes. Further, ice nucleation followed Cooper (1986).

1.2 Experiment design

1.2.1 Number of predicted moments

A first set of experiments is designed to understand whether a two-moment approach is necessary for all precipitating hydrometeors, or whether a one-moment approach is sufficient to simulate the essential features associated with deep convection. A first experiment implemented the fully two-moment versions of the MTT and the MY schemes (MTT-BASE and MY-BASE). Subsequent experiments consisted of modifying, one by one, the representation of precipitating hydrometeors to only predict one moment of their respective distributions. First, graupel number concentration was diagnosed instead of predicted, while rain and snow number concentrations were still explicitly predicted (MTT-2R2S1G and MY-2R2S1G). Second, both snow and graupel number concentrations were diagnosed, yet rain number concentration was still predicted (MTT-2R1S1G and MY-2R1S1G). Finally, both schemes were made fully one-moment for each of the hydrometeors (MTT-1R1S1G and MY-1R1S1G), except for cloud ice and cloud water, which remained two-moment in all experiments. The implementation of a one-moment approach for

each specie requires the specification of the intercept N_{0X} of the size distribution (equation 1). Table 2 lists the values for N_{0X}, as well as the density applied for each specie.

1.2.2 Number and nature of predicted ice categories

A second set of experiments investigates the impact of increasing the number of precipitating ice categories to three. In order to do so, we extended the fully two-moment versions of both microphysics schemes as described above (MTT-BASE and MY-BASE) to also include hail along with graupel (MTT-GH and MY-GH). The implementation of an additional ice category requires several additional conversion terms. In the original formulations of Milbrandt and Yau (2005), graupel and hail were present and we applied the MY scheme accordingly for the MY-GH experiment. For the MTT-GH experiment, the collection by hail of cloud water, rain and snow was implemented according to the formulations of collection of these categories by graupel in the MTT-BASE scheme. Further, freezing of rain drops was added as a source term for hail (not graupel), and the conversion of graupel to hail was implemented as described in Milbrandt and Yau (2005). For the three-category interactions that can result in graupel or hail (i.e., collection of rain by graupel and cloud ice by rain), parameterization is done based on the resulting bulk density of the destination particle, consistent with Milbrandt and Yau (2005). Further, we implemented a size threshold of 5.0 mm below which hail would be converted back to graupel in the MTT-GH experiment, consistent with the original formulation of the MY-GH scheme.

An additional experiment was performed with only two precipitating ice categories, but including hail along with snow, instead of graupel (MTT-H and MY-H). Constants for the m-D and V-D relationships for these experiments are provided in Table 1.

1.2.3 Conversion process formulations

A last set of experiments was designed to examine the role of the conversion term formulations in order to understand why the MTT-BASE and MY-BASE schemes still yield considerable differences in their representation of moist processes and surface precipitation despite their similar level of complexity (Morrison and Milbrandt 2011). The microphysical conversion processes were divided into three groups, being "warm rain processes", "ice deposition and initiation processes", and "collection processes". Each of these three groups of processes was investigated by making the conversion terms that comprise them equal in both schemes. The MTT-BASE scheme was arbitrarily chosen as the scheme that was gradually modified by implementing the formulations of the MY-BASE scheme, until both schemes were identical.

First, the warm rain scheme based on Cohard and Pinty (2000), as used in MY, was implemented in the MTT-BASE scheme (MTT-WM). A second experiment consisted of additionally implementing all processes associated with precipitating and non-precipitating ice initiation, deposition and other conversion of the MY scheme into the MTT-WM scheme (MTT-WM-ICE). Last, the MTT-WM-ICE scheme was further modified with the collection terms and efficiencies from the MY scheme (MTT-WM-ICE-COL) and hence was basically identical to the MY-BASE scheme. A detailed description of which processes were changed in each of these experiments is provided in Appendix A. An overview of all experiments and their specifications is provided in Table 3.

2. Results

2.1 Number of predicted moments

Figure 1 shows vertical cross sections of the radar reflectivity for both the MTT-BASE and the MY-BASE simulations, showing a well-formed squall line in both simulations. Associated 5 hour-accumulated surface precipitation characteristics for all experiments can be found in Tables

4 and 5 and are visualized in Figure 2. None of the experiments on the number of predicted moments led to surface precipitation changes beyond 15% as compared to the baseline simulations (MTT-BASE and MY-BASE), which is consistent with Morrison et al. (2009). Microphysics can affect surface precipitation generally in two possible ways. First, microphysics schemes have different ways of handling the transition from the available water vapor supersaturation over the different slow (e.g., cloud water) or fast (e.g., hail) hydrometeors to fallout as rain to the surface. Some microphysics schemes tend to favor formation of slow precipitation or have more intense re-evaporation of condensate; others favor a fast fallout of precipitation. A measure to quantify this effect is the precipitation efficiency (PE), defined here following Sui et al. (2005):

$$PE = \frac{P}{vapor\ loss} \qquad (4)$$

where P is the domain total surface precipitation (kg), and "vapor loss" is all vapor consumed by the microphysics parameterization across the same domain (kg), being cloud water condensation, graupel, snow and ice deposition and ice initiation from vapor. A second possible way microphysics schemes affect the surface precipitation is by interacting with the dynamics, by the release of large amounts of latent heat associated with condensation or freezing processes or by affecting cold-pool development. In order to determine whether differences in surface precipitation between the different experiments are predominantly due to the former or the latter effect, Tabled 4 and 5 provide the precipitation efficiency (PE) (more directly related to microphysics) and the domain-average updraft latent heat release for each experiment (more related to microphysics-dynamics interaction).

Implementing a two-moment formulation for rain (MTT-2R1S1G and MY-2R1S1G), as opposed to a one-moment formulation (MTT-1R1S1G and MY-1R1S1G), does not significantly

affect surface precipitation, PE, latent heat (Table 4 and 5), or the vertical hydrometeor profiles (Figure 3), although a slight increase in the domain-maximum precipitation occurs. This increase in domain-maximum precipitation is more pronounced in the MY-2R1S1S experiment. Figure 4 provides time-averaged vertical profiles of rain mixing ratio, drop size and evaporation associated with the location of the largest surface-precipitation accumulation. Obviously, predicting the number concentration of rain explicitly allows size sorting of drops to take place. On average across the domain, this leads to smaller drops aloft and larger drops near the surface, which has little effect on total rain evaporation (Figure 3). However, in the region with heavy precipitation, rain drops grow larger very rapidly as they are falling, leading to decreased evaporation and more precipitation at the surface (Figure 4). The reason for differences in the impact of this experiment between the MY and the MTT scheme is probably related to the more active drop breakup parameterization in the latter scheme, as shown in Morrison and Milbrandt (2011).

In the MTT experiments, an increase in PE occurs when going from one-moment snow (MTT-2R1S1G) to two-moment snow (MTT-2R2S1G). This is associated with significant changes in the snow sizes (Figure 3). Two-moment snow better reproduces the size sorting of large snowflakes on their way to the surface. These larger snowflakes fall out more quickly, reducing the snow content in the mid-troposphere (Figure 3). Furthermore, the two-moment approach also explicitly reproduces aggregation of snow flakes, further leading to larger snowflakes at lower altitudes. It should be mentioned that one-moment schemes implementing a temperature-dependent N_{0S}, rather than a fixed N_{0S} as in our simulations, also tend to better reproduce the larger snow sizes near the freezing level (e.g., Thompson et al. 2004). Figure 5 helps interpret the changes in PE among the different experiments. For a unit amount of condensation and deposition across the domain and the full time integration, this figure shows

the amount of condensate that is returned to the vapor phase. It is clear that the quicker fallout of snow permits less time for sublimation (Pvsbs) hence leading to increased PE. However, less latent heat is released in the updrafts as well (due to lower depositional growth), which offsets the higher PE. As snow is far less abundant in the MY scheme (Figure 3), size sorting and aggregation of snow hardly affects the simulation and hence there is little difference between MY-2R1S1G and MY2R2S1G. Domain-maximum precipitation accumulations increased slightly in MY-2R2S1G and MTT-2R2S1G experiments, due to increased rain mixing ratios (Figure 4).

A drop of 15 to 20% in latent heat release occurs in the MTT-BASE and the MY-BASE experiments compared to the MTT-2R2S1G and MY-2R2S1G experiments, leading to a reduction in domain-average precipitation (Table 4 and 5). Figure 2 reveals that this reduction in precipitation occurs mainly in the region of lighter precipitation in front of the squall line, while the more heavy precipitation in the convective cores is enhanced. In order to explain this behavior, it is instructive to look at the cold-pool dynamics. Cold pools originate mainly from evaporating rain that impact the dynamics of storms (Rotunno et al. 1988, Weisman and Rotunno 2004). Figure 6 shows the time evolution of the cold pools for the experiments on the number of predicted moments. In the MTT scheme, it is not until graupel number concentration becomes prognostic that the mean and maximum cold-pool intensity decreases. In the MY scheme however, both prognostic rain and graupel number concentrations weaken the cold pools. The different behavior of the MTT and MY schemes, as the number concentration of rain is predicted, can probably be attributed to differences in the collisional breakup formulations, as suggested by Morrison and Milbrandt (2011). The more active breakup in MTT seems to eliminate the impact of rain drop size sorting to some extent (larger drops are broken up more readily), which apparently is not the case in the MY scheme.

The behavior of both schemes as graupel number concentration is explicitly predicted can be explained by Figure 3. This figure shows that in the MTT-BASE and the MY-BASE schemes, intense graupel size sorting takes place that leads to larger graupel particles below the freezing level. Since melting graupel is the main source for rain, the larger graupel particles also melt into larger rain drops (Figure 3), which effectively reduces the rain evaporation and cold-pool intensity. Furthermore, as graupel is larger upon its melting, melting of graupel will also be slower, further reducing the cooling rates. Previous research has indicated the impact of two prognostic moments for rain on cold-pool development (Dawson et al. 2010, Morrison et al. 2009), but our simulations suggest that prognostic graupel number concentration also strongly affects the cold pool intensity. The impact of graupel size sorting on the rain size distribution is also clear from Figure 7, showing vertical cross sections through the squall line. This figure also gives a hint as to why surface precipitation in front of the squall line was reduced within the MTT-BASE and MY-BASE experiments compared to the experiments with one-moment graupel (MTT-2R2S1G and MY-2R2S1G). The larger evaporation of the smaller rain drops in the experiments with one-moment graupel causes stronger cold outflows behind the gust front of the squall line. In the MTT-2R2S1G experiment, this strong outflow generates gravity waves leading to the development of new cells in front of the squall line (compare Figures 7a and 7b). In the MTT-BASE experiment, the outflow seems to be too weak to do so and hence, less precipitation accumulates in front of the squall line. No clear cell regeneration in front of the squall line occurs in the MY-2R2S1G experiment, but even in this case, stronger outflow in the MY-2R2S1G experiments enhances squall line propagation compared to the MY-BASE experiment, leading to a broader precipitation swath (Figure 7a and 7b). From Figure 6, this also leads to smaller cold pool area in the baseline experiments as compared to the experiments with one-moment graupel (MTT-2R2S1G and MY-2R2S1G). This is consistent with the Van Weverberg et al. (2011b) simulations of supercell storms, where the cold-pool areas were more confined when a less

evaporation-friendly rain size distribution was applied. However, since generally less rain evaporates as well (Figure 5), PE and maximum-precipitation accumulation increase in our simulations.

2.2 Nature and number of predicted ice categories

A number of previous studies stated that surface precipitation is mainly sensitive to the nature of the rimed precipitating ice species (either graupel or hail) within bulk microphysics schemes (Gilmore et al. 2004, van den Heever and Cotton 2004, Morrison and Milbrandt 2011, Bryan and Morrison 2011). If the rimed precipitating species were large hail, surface precipitation could increase by as much as 30% (van den Heever and Cotton 2004) and up to 300% (Gilmore et al. 2004) as compared to identical simulations where the largest precipitating ice specie was small graupel. However, most of these studies were performed for 3D supercell simulations and, hence, were based on rather short simulations (about 2 hours). Therefore we investigated whether these conclusions still held for squall lines and when simulations were integrated over longer time scales.

From Tables 4 and 5 and Figure 8, the inclusion of hail (MTT-H and MY-H) as opposed to graupel (MTT-BASE and MY-BASE) leads the domain-average precipitation to be only slightly higher after 5 hours of simulation. In the MTT-H experiment, the 15 % increase in precipitation is due to both a slightly higher PE and latent heat release as compared to the MTT-BASE experiment. In the MY-H experiment, however, the slight precipitation enhancement (7 %) is only due to higher updraft latent heat release. PE is reduced significantly compared to the MY-BASE experiment. The reason for this can be found in the differences in the domain-average vertical profiles of hydrometeor mixing ratio (Figure 9). It is clear that, while a slight increase in snow mixing ratio occurs in the MTT-H experiment, the MY-H experiment produces as much as five times the amount of snow compared to the MY-BASE experiment. Figure 10 provides the

amount of vapor returned by the microphysics, normalized over the total condensation and deposition for each experiment, which is helpful to interpret the changes in PE. The strong growth in snow amounts in the MY-H experiment leads to a strong increase in snow sublimation outside the updraft cores. This increased return of vapor from the condensate effectively reduces PE compared to MY-BASE. Enhanced latent heat release can again be associated with differences in cold pool strengths. Figure 11 reveals that cold pools are considerably larger and more intense in the experiments with large hail as opposed to graupel; melting hail contributes to the latent cooling down to the surface, whereas graupel quickly melts below the melting level. Stronger and deeper cold pools again seem to enhance the outflow, providing additional dynamical forcing for updrafts and increasing the latent heat release (Tables 4 and 5). Domain-maximum precipitation is about 40% larger after 5 hours of simulation in the MTT-H experiment compared to MTT-BASE, while a decrease occurs in the MY-H experiment (Tables 4 and 5 and Figure 8) compared to MY-BASE. It should be mentioned that differences in surface precipitation between the baseline simulations and the simulations including hail were larger earlier into the simulations. Domain average precipitation (domain maximum precipitation) was typically 40 – 60 % (100 – 200 %) larger in the simulations with hail compared to the baseline simulations 2 hours into the simulations (not shown).

Further, we investigated the influence of adding ice categories to the simulations by extending the MTT and MY schemes to include both graupel and hail. This was suggested by, for example, McCumber et al (1991) and Cohen and McCaul (2006) in order to make simulations of convective storms more realistic. The inclusion of both hail and graupel (MTT-GH and MY-GH) has a rather insignificant impact on surface precipitation compared to simulations that only contain graupel (MTT-BASE and MY-BASE). A slight decrease in surface precipitation in both schemes is associated with a decrease in PE and an increase in latent heat.

From the vertical profiles of the hydrometeors in Figure 9, it is clear that the main impact of including both graupel and hail consists of an increase in the graupel number concentration. In the MTT-GH experiment, this effectively increases riming growth of graupel at the expense of snow riming growth (not shown), leading to an increase in graupel mixing ratios and a decrease in snow mixing ratios. Further, higher graupel number concentration leads to greater depositional growth, significantly increasing the latent heat release by over 30% (Table 4). However, the more numerous graupel particles are also more prone to sublimation (mainly outside the convective cores) and, hence, more condensate is returned to the vapor phase. In combination with the much slower fallout by the smaller particles, this dramatically reduces the PE. As the more numerous graupel particles also affect the rain size distribution upon melting, PE is further reduced due to enhanced rain evaporation (Figure 10). In the MY-GH experiment, graupel deposition/sublimation and the associated latent heat release are not parameterized. Hence the dramatic impact of the more numerous particles on deposition and sublimation does not occur in this case. The higher number concentration of graupel still leads to smaller rain drops and more evaporation, however, and hence PE is reduced also in this experiment as compared to MY-BASE (Table 5 and Figure 10). As in the MTT-GH experiment, this is counterbalanced by a larger latent heat release (Table 5), which might be associated with deeper cold pools connected to the enhanced rain evaporation in this case (Figure 11). The larger evaporation of rain and the smaller, slower-falling rain drops also cause the domain-maximum precipitation accumulation to decrease by 20% in the MTT-GH and the MY-GH experiments compared to baseline (Tables 4 and 5).

Differences in the vertical profiles of graupel and hail between our graupel-only, hail-only and graupel plus hail experiments resemble those found by Morrison and Milbrandt (2011) for their experiments on the impact of graupel and hail on the simulation of an idealized 3D

supercell. Vertical profiles of hail (Figure 9) reveal that although both hail and graupel processes are parameterized, hardly any hail occurs. This also makes the MTT-GH and the MY-GH resemble their counterparts that have only graupel. The main reason for this lack of hail is that in both schemes a size threshold of 5 mm is implemented, below which hail is converted back to graupel at every time step. This effectively prevents hail from growing. In order to investigate the impact of this threshold, an additional experiment was carried out with both hail and graupel but without the threshold that converts hail back to graupel (MTT-GH-NT and MY-GH-NT). As far as surface precipitation is concerned, the removal of this threshold makes the experiments with both hail and graupel resemble more closely the hail-weighted experiments (MTT-H and MY-H). Graupel number concentration in the experiments without the graupel/hail threshold is not enhanced as dramatically as in the experiments with such threshold (Figure 9). Therefore, graupel deposition and sublimation, as well as the latent heat release associated with it, do not increase as much in the MTT-GH-NT experiment. Since graupel deposition and sublimation are not parameterized in the MY-GH experiment, the impact of removing the threshold is less obvious. Latent heat release increases somewhat in the MY-GH-NT experiment. This is probably associated with the more intense cold pools, as large hail reaches the surface. The probable reason for larger graupel number concentration in the experiments with the graupel/hail threshold (MTT-GH and MY-GH) is that a considerable number of hailstones are produced at every time step in these experiments, which are subsequently converted to graupel as long as the hail size remains small enough. Since graupel tends to sediment much slower than hail, this eventually leads to large accumulation of graupel particles aloft. From the vertical profiles (Figure 9), it becomes clear that hail and graupel co-exist in equally large quantities in the MTT-GH-NT and MY-GH-NT experiments. Since the behavior of these experiments is more like the hail-only experiments, domain maximum precipitation is also enhanced (Table 4 and 5).

2.3 Conversion process formulations

As described in section 3.1, the MTT and MY schemes exhibit very different behavior in terms of surface precipitation characteristics (Tables 4 and 5). Typically, MY produces 20 to 30% more surface precipitation, while the precipitation extremes are twice as large. Previous sections have shown that one of the key differences between the schemes is that MY tends to favor riming, while MTT tends to favor depositional growth (for this idealized case). Since the latent heat released by deposition is about an order of a magnitude larger than that associated with riming, this leads to more latent heat being released in MTT (Table 4). Indeed, while latent heating associated with depositional growth (riming growth) accounts for 30% (7%) of the total latent heat released within updrafts in the MTT scheme, this drops to about 7% (9%) in the MY scheme (almost all other latent heat release is due to condensation). This accounts for a 10 to 20% larger latent heat release in the MTT scheme. On the other hand, Tables 4 and 5 also show that PE is typically 30 to 60% larger in the MY scheme, mainly associated with less condensate being returned to vapor by sublimation processes outside the updraft cores. Recall that less snow is present in the MY scheme (and hence less snow sublimation occurs) and graupel deposition/sublimation is not parameterized in this scheme. The net effect of a much higher PE and a slightly lower latent heat in the MY scheme is an increase in surface precipitation. In order to further understand the origin of these differences, a series of experiments gradually replaced the formulations of the MTT scheme by those of the MY scheme.

The first experiment consisted of implementing the warm rain scheme of MY into MTT (MTT-WM). Details of the particular modifications that were made in this experiment are listed in the Appendix (e.g., melting of graupel and snow were also modified in this experiment). Apparently, the warm rain scheme does not have much of an impact on the domain average precipitation, although it is responsible for the difference in domain-maximum precipitation

between the MY and the MTT schemes (Table 4 and Figure 12). Domain-maximum precipitation goes up by nearly 80%, which is close to the value obtained in MY. One of the differences between the warm rain formulations of both schemes is the representation of collisional drop breakup. Both schemes follow Verlinde and Cotton (1993) to calculate the combined effect of rain self-collection and collisional drop breakup:

$$\left.\frac{dN_R}{dt}\right|_{self+brk} = -EC * NRAGR \quad (5)$$

where *NRAGR* represents rain self-collection and *EC* is the collection efficiency defined as:

$$EC = \begin{cases} 1, & D_{NR} < Thr \\ 2 - \exp(2300 * (D_{NR}) - Thr), & D_{NR} \geq Thr \end{cases} \quad (6)$$

As soon as the number weighted mean drop diameter D_{NR} grows larger than a threshold diameter *Thr*, *EC* becomes smaller than 1 and starts to counterbalance the number of raindrops lost by self-collection. Hence, collisional drop breakup is represented implicitly by increasing the number concentration of raindrops. While MY applies a *Thr* of 600 μm, MTT applies a lower value of 300 μm, leading to more intense breakup in MTT.

In order to understand the sole impact of drop breakup, an additional experiment was performed, identical to the MTT-WM experiment, but leaving the collisional drop breakup as in the original MTT experiment (MTT-WM-BRK). From Table 4, this experiment has little impact on domain-average precipitation, consistent with Morrison and Milbrandt (2011). On the other hand, this experiment brings the domain-maximum precipitation back to the value obtained in the MTT-BASE experiment, indicating that collisional drop breakup is the main factor determining the differences in peak precipitation between the schemes. Figure 13 shows the vertical profiles of rain mixing ratio, drop size, and evaporation that are associated with the location of maximum-domain-precipitation accumulation. Clearly, the lower threshold used for

drop breakup in the MTT scheme limits the size of the largest drops to be much smaller than those in MY, leading to slower fallout. It should be noted that the vertical profile of rain mixing ratio in the MTT-WM-BRK experiment is not entirely the same as in the MTT-BASE experiment. Larger mixing ratios are present aloft in the MTT-WM-BRK experiment, but since rain evaporation is larger, the eventual fallout to the surface becomes similar for these two experiments (Figure 13). In the MTT-WM experiment, rain evaporation is similar to the MTT-BASE experiment, despite much larger mixing ratios, because of the presence of larger rain drops. The increase of peak surface precipitation in the MTT-WM experiment seems to be compensated by a reduction in surface precipitation in the frontal area of the squall line, possibly due to slower propagation (Figure 12), yielding no significant impact on the domain-average precipitation (Table 4). This might be related to the more vigorous outflow generating cells near the gust front in the MTT-BASE experiment. Indeed, the smaller drops associated with the different breakup formulation in MTT-WM-BRK favors more evaporative cooling. Figure 14 shows that the MTT-WM experiment is also associated with a reduction in snow mixing ratios. This was found to be associated with differences in cloud activation between the schemes (not shown). The MTT scheme typically produces larger cloud number concentrations than the MY scheme, mainly in the lower atmosphere, which seems to favor graupel riming growth at the expense of snow riming growth.

The second step toward unraveling the differences between the MY and the MTT schemes consisted of additionally replacing the formulations dealing with deposition growth and ice-to-snow autoconversion in MTT-WM with those of MY (MTT-WM-ICE). This experiment leads to a significant increase in domain-average surface precipitation of about 20%, while the domain maximum increases by 10%. The surface precipitation enhancement is associated with a 20% increase in PE. The main reason for this increase is the absence of graupel

deposition/sublimation in the MY scheme (and hence in the MTT-WM-ICE experiment). This is also clear from Figure 15, which shows the normalized total amount of water vapor returned by microphysical processes for all of the conversion term formulation experiments. Graupel sublimation returns significant amounts of condensate back to the vapor phase in the MTT-BASE experiment, which lowers the PE. Not implementing the sublimation of graupel leads to higher PE and also larger precipitation fallout. It can be seen that the spatial distribution of accumulated precipitation in Figure 12 is broadened in the MTT-WM-ICE experiment. Furthermore, PE in the MTT-WM-ICE experiment increases further due to less snow depositional growth (Figure 15), which is associated with the less-active snow deposition formulation used in MY as compared to the formulations of Harrington et al. (1995) used in MTT. Figure 16 shows the impact of each of the conversion term formulation experiments on the sinks and sources of the snow mixing ratio. It is clear that the reduction in snow depositional growth is partly compensated by more ice-to-snow autoconversion in the MTT-WM-ICE experiment, which leads to a rather minor change in the snow mixing ratios.

The last step in systematically converting the MTT scheme into the MY scheme consisted of implementing the collection growth formulations of MY in the MTT-WM-ICE experiment (MTT-WM-ICE-COL). This slightly reduces the domain-average and maximum precipitation, bringing those values in close agreement with the MY scheme (Tables 4 and 5). Graupel growth in this experiment is favored further at the expense of snow growth, which reduces the snow mixing ratios to the amounts in the MY experiment (Figure 14). This is also clear from Figure 16, indicating that only autoconversion from cloud ice and depositional growth remain significant growth terms for snow. Graupel mixing ratio does not increase due to a larger downward flux associated with the smaller number concentration. The reduction in snow amount further reduces the amount of condensate that can sublimate back to the vapor phase and, hence,

further enhances PE. However, latent heat release is decreased as well, leading to a small reduction in domain-average surface precipitation. The reason for the differences in snow mixing ratios between the MY and the MTT schemes, hence, seems to be a combination of factors, including differences in cloud activation, snow depositional growth and collection efficiencies.

3. Discussion and conclusions

A challenge to learning from comparisons of deep convection simulations with observations is a lack of understanding for the reasons for variability among different models. If it is unknown why equally complex models can exhibit substantially different behavior in terms of surface precipitation, it is hard to provide sound recommendations to model developers as to which aspects of the models require improvement. It is also often vaguely understood how additional complexity in models affects the details of their behavior. In order to address these issues, this work examined the role of adding complexity to microphysics schemes in idealized squall-line simulations within the framework of two commonly used two-moment bulk microphysics schemes.

We have shown that the explicit prediction of the number concentration for *all* precipitating hydrometeors is crucial since many important physical features, such as size sorting, cannot take place without it. Size sorting allows the mean-particle diameter to be larger during sedimentation towards the surface, which makes the particles less prone to evaporation and thus enhances surface precipitation. This was found to impact precipitation extremes. In contrast to many previous studies, we found that the explicit treatment of graupel number concentration was important to reducing cold-pool development. Size sorting allowed the largest graupel particles to accumulate around the freezing level and subsequently melt into larger raindrops that were less prone to evaporation. Thus cold-pool intensity was significantly reduced mainly when two-moment rain was combined with a two-moment graupel treatment. A 10 to 15% decrease in

surface precipitation in the two-moment graupel experiments can be associated with the weaker cold outflow, which slows down squall line propagation and prevents cell generation from taking place in front of the squall line.

Second, compared to many previous studies, we found a smaller sensitivity of surface precipitation to the representation of the rimed ice species (graupel or hail). It is uncertain at this time whether the reason for the difference is because most of the previous research dealt with idealized simulations of supercells, or whether it is due to the fact that those simulations were rather short. Bryan and Morrison (2011) also found somewhat larger sensitivity of precipitation (up to 30% more precipitation when the rimed species was hail) for their 9-hour simulations of idealized squall lines as compared to our simulations (15% more precipitation when the rimed species was hail). Simulations where both hail and graupel were included showed that adding ice categories does not have a very large impact on domain-average surface precipitation behavior, although domain-maximum precipitation was decreased by 20%. It was found, however, that simulations containing both hail and graupel are sensitive to the threshold that determines the minimum size for hail to be sustained. The hail that is produced by these simulations typically is too small to be sustained and hence is converted back to graupel. While the basis of this threshold is that hail embryos are typically larger than 5 mm, the scheme seems to be too stringent on hail initiation. Further, the way the threshold is implemented allows duplication of several production terms for graupel, leading to large graupel mixing ratios and number concentrations. Simulations swing in behavior between the graupel-only experiments and the hail-only experiments depending on the application of the threshold. This finding indicates a need for a more physical treatment of the graupel-to-hail conversion.

Last, we have shown what causes the different behavior in terms of surface precipitation and moist processes aloft in the MTT and the MY schemes, given identical size distribution

assumptions and number of ice categories. While the MTT scheme was identified as a deposition-dominated scheme (more snow) with low precipitation efficiency, MY was found to be dominated by riming process (more graupel) with high precipitation efficiency. MTT typically produced up to 30% less domain-average precipitation, while the peak precipitation was only 50% of what MY produced. The lower precipitation efficiency in the MTT scheme was found to be associated mainly with graupel deposition/sublimation, which is not parameterized in the MY scheme. A recommendation to model developers would be to include the sublimation of graupel in microphysics schemes, since it might return significant amounts of condensate to the vapor phase outside of the convective cores, reducing the precipitation efficiency. The absence of graupel sublimation in the MY scheme, and hence the higher precipitation efficiency, was the main factor responsible for the differences in domain-average surface precipitation between the MTT and the MY schemes. Domain-maximum precipitation differences, however, were almost entirely due to the different treatments of collisional drop breakup between the schemes. Breakup in the MTT scheme occurs at drop sizes only half as those in the MY scheme. Due to the smaller drops in the region of heavy precipitation in the MTT scheme, domain-maximum-accumulated precipitation was found to be much smaller compared to the MY scheme. Differences in terms of snow amount aloft between the schemes were associated with an amalgam of processes, including cloud activation, snow depositional growth and collection efficiencies.

In this research we have pointed to the importance of rain drop sizes and evaporation rates on surface precipitation. Therefore, a strong need exists for observational data on vertical profiles of rain mixing ratio and drop sizes in order to determine better approaches for microphysics modeling. Over the past years, the focus in microphysics modeling often has been on the role of size distribution assumptions on moist processes and surface precipitation (e.g., bulk vs. spectral approaches, graupel vs. hail, two-moment vs. one-moment), but it is clear that an equally large

variability is introduced by differences in the microphysical conversion term formulations. Thus, we recommend that improved formulations of collection, deposition and melting, based on laboratory experiments and field campaigns, should be one of the primary foci for model improvement over the next years.

4. Acknowledgements

We thank Wuyin Lin and Yangang Liu for stimulating discussions. The research by K. Van Weverberg and A. M. Vogelmann was supported by the U.S. Department of Energy's Atmospheric Science Program Atmospheric System Research, an Office of Science Office of Biological and Environmental Research program, under contract DE-AC02-98CH10886. Hugh Morrison was supported by U.S. DOE ARM DE-FG02-08ER64574, NOAA grant NA08OAR4310543, and by the NSF Science and Technology Center for Multiscale Modeling of Atmospheric Processes (CMMAP) managed by Colorado State University under cooperative agreement ATM-0425247. We also thank Amy Solomon for providing the code on cloud activation in the MTT scheme. National Center for Atmospheric Research is sponsored by the National Science Foundation.

5. Appendix

5.1 Conversion Term Experiments

The following conversion term formulations in MTT were modified to match to those in MY in each of the respective experiments (Abbreviated conversion term formulations are explained in appendix 6.2):

- MTT-WM: All conversion terms associated with warm rain processes as well as all melting processes (Pvevr, Pwcdv, Pvevw, Pracw, Prauw, Psmlt, Pimlt, Pgmlt, breakup and cloud activation)
- MTT-WM-BRK: as in MTT-WM, but with breakup formulated as in the MTT scheme (breakup threshold of 300 μm)
- MTT-WM-ICE: as in MTT-WM, but also all processes associated with deposition and solid autoconversion (Pgdpv, Pvsbg, Psdpv, Pvsbs, Pidpv, Pvsbi, Psaui, Pintv, Pifrw, Pgaus)
- MTT-WM-ICE-COL: as in MTT-WM-ICE, but also all collection terms

5.2 Conversion Term Abbreviations

All abbreviations are constructed so that the second (last) letter is the category experiencing the gain (loss). The third and fourth letter indicate the process associated with the conversion: ev (evaporation), cd (condensation), sb (sublimation), dp (deposition), ac (accretion), nt (initiation), au (autoconversion), fr (freezing). When three categories are involved, the third letter indicates the category not experiencing any loss or gain.

Pvevr	Rain evaporation
Pvsbi	Cloud ice sublimation
Pvsbg	Hail / graupel sublimation
Pvsbs	Snow sublimation
Pvevw	Cloud water evaporation
Pwcdv	Cloud water condensation
Pidpv	Cloud ice depositional growth at the expense of water vapour
Psdpv	Snow depositional growth
Pintv	Initiation of cloud ice at the expense of water vapour
Psaui	Autoconversion of cloud ice to snow
P(g)(s)raci	Collection of cloud ice by rain adding to hail / graupel or snow (loss term for cloud ice)
P(g)(s)iacr	Collection of rain by cloud ice adding to hail / graupel or snow (loss term for rain)
Pgaci	Collection of cloud ice by hail / graupel
Prauw	Autoconversion of cloud water to rain
P(r)sacw	Collection of cloud water by snow adding to rain or snow
Pracw	Collection of cloud water by rain
Pgacw	Collection of cloud water by hail / graupel
Prgacw	Collection of cloud water by hail / graupel adding to rain
Psaci	Collection of cloud ice by snow
Ps(g)acr	Collection of rain by snow adding to hail / graupel or snow
Pgacs	Collection of snow by hail / graupel
Pgaus	Autoconversion of snow to hail / graupel
Pgracs	Collection of snow by rain adding to hail / graupel
Prmls	Melting of snow to rain
Pgacr	Collection of rain by hail / graupel
Pgfrr	Homogeneous freezing of rain to hail / graupel
Prmlg	Melting of hail / graupel to rain

6. References

Bryan, G.H., H. Morrison, 2011: Sensitivity of a simulated squall line to horizontal resolution and parameterization of microphysics. *Mon. Weather. Rev*., submitted.

Cohard, J.M., J.P. Pinty, 2000: A comprehensive two-moment warm microphysical bulk scheme. I: Description and tests. *Q. J. R. Meteorol. Soc*., **126**, 1815-1842.

Cohen, C., McCaul Jr., E. W., 2006: The sensitivity of simulated convective storms to variations in prescribed single-moment microphysics parameters that describe particle distribution sizes and numbers. *Mon. Weather. Rev*., **134**, 2547-2565.

Cooper, W.A., 1986: Ice initiation in natural clouds. Precipitation Enhancement – A scientific challenge, *Meteor. Monogr*., **43**, Amer. Meteor. Soc., 29-32.

Cotton, W.R., M.A.Stephens, T. Nehrkorn, G.J. Tripoli, 1982: The Colorado State University three-dimensional cloud/mesoscale model-1982. Part II: An ice phase parameterization. *Journal de Researches Atmospheriques*, **16**, 295-320.

Dawson, D.T., M. Xue, J.A. Milbrandt, M.K. Yau, 2010: Comparison of evaporation and cold-pool development between single-moment and multimoment bulk microphysics schemes in idealized simulations of tornadic thunderstorms. *Mon. Weather. Rev*., **138**, 1152-1171.

Ferrier, B. S., 1994: A double-moment multiple-phase four-class bulk ice scheme, Part I: description. *J. Atmos. Sci.*, **51**, 249-280.

———, W.-K. Tao, J. Simpson, 1995: A double-moment multiple-phase four-class bulk ice scheme. Part II: Simulations of convective storms in different large-scale environments and comparison with other bulk parameterizations. *J. Atmos. Sci*., **52**, 1001-1033.

Gilmore, M. S., Straka, J. M., Rasmussen, E. N., 2004: Precipitation uncertainty due to variations in precipitation particle parameters within a simple microphysics scheme. *Mon. Weather. Rev.*, **132**, 2610-2627.

Harrington, J.Y., M.P. Meyers, R.L. Walko, W.R. Cotton, 1995: Parameterization of ice crystal conversion processes due to vapour deposition for mesoscale models using double-moment basis functions. Part I: Basic formulation and parcel model results. *J. Atmos. Sci*., **52**, 4344-4366.

Kessler, E., 1969: On the distribution and continuity of water substance in atmospheric circulations. *Meteor. Momogr*., **32**, Amer. Meteor. Soc., 84 pp.

Lin, Y.- L., Farley, R. D., Orville, H. D., 1983: Bulk parameterization of the snow field in a cloud model. *J. Clim. Appl. Meteorol.*, **22**, 1065-1092.

Locatelli, J. D., Hobbs, P. V., 1974: Fall speeds and masses of solid precipitation particles. *J. Geophys. Res*., **79**, 2185-2197.

McCumber M., Tao, W.- T., Simpson, J., Penc, R., Soong, S.- T., 1991: Comparison of ice-phase microphysical parameterization schemes using numerical simulations of tropical convection. *J. Appl. Meteorol*., **30**, 985-1004.

Milbrandt, J. A., Yau, M. K., 2005: A multimoment bulk microphysics parameterization. Part II: A proposed three-moment closure and scheme description. *J. Atmos. Sci*., **62**, 3065–3081.

———, ————, 2006: A multimoment bulk microphysics parameterization. Part III: Control simulation of a hailstorm. *J. Atmos. Sci*., **63**, 3077–3090.

Morrison, H., G. Thompson, V. Tatarskii, 2009: Impact of cloud microphysics on the development of trailing stratiform precipitation in a simulated squall line: Comparison of one- and two-moment schemes. *Mon. Weather, Rev*., **137**, 991-1007.

———, J. Milbrandt, 2011: Comparison of two-moment bulk microphysics schemes in idealized supercell thunderstorm simulations. *Mon. Weather. Rev.,* (in press).

Rutledge, S. A., Hobbs, P. V., 1983: The mesoscale and microscale structure and organization of clouds and precipitation in mid-latitude cyclones. Part VIII: A model for the "seeder-feeder" process in warm-frontal rainbands. *J. Atmos. Sci*., **40**, 1185-1206.

Rotunno, R., J.B. Klemp, M.L. Weisman, 1988: A theory for strong, long-lived squall lines. *J. Atmos. Sci*., **45**, 463-485.

Seifert, A., Beheng, K. D., 2001: A double-moment parameterization for simulating autoconversion, accretion and self-collection. *Atmos. Res*., **59-60**, 265-281.

Skamarock, W.C., J.B. Klemp, J. Dudhia, D.O. Gill, D.M. Barker, W. Wang, J.G. Powers, 2007: A description of the Advanced Research WRF Version 2. *NCAR technical note NCAR/TN-468+STR*.

Straka, J.M., E.R Mansell, 2005: A bulk microphysics parameterization with multiple ice precipitation categories. *J. Appl. Meteorol*., **44**, 445-466.

Sui, C. H., X. Li, M.- J. Yang, 2007 : On the definition of precipitation efficiency. *J. Atmos. Sci*., **64**, 4506-4513.

Thompson, G., R.M. Rasmussen, K. Manning, 2004: Explicit forecasts of winter precipitation using an improved bulk microphysics scheme. Part I: Description and sensitivity analysis. *Mon. Weather. Rev.,* **132**, 519-542.

Tripoli, G.J., W.R. Cotton, 1980: A numerical investigation of several factors contributing to the observed variable intensity of deep convection over South Florida. *J. Appl. Meteorol*., **19**, 1037-1063.

van den Heever, S.C., W.R. Cotton, 2004: The impact of hail size on simulated supercell storms, *J. Atmos. Sci*., **61**, 1596-1609..

Van Weverberg, K., N.P.M. van Lipzig, L. Delobbe, 2011a: The evaluation of moist processes in km-scale NWP models using remote sensing and in-situ data: Impact of size distribution assumptions. *Atmos. Res.,* **99**, 15-38.

———, ———, ———, 2011b: The impact of size distribution assumptions in a simple microphysics scheme on surface precipitation and storm dynamics during a low-topped supercell case. *Mon. Weather. Rev.,* (in press).

Verlinde, H., W.R. Cotton, 1993: Fitting microphysical observations of nonsteady convective clouds to a numerical model: An application of the adjoint technique of data assimilation to a kinematic model. *Mon. Weather Rev*., **121**, 2776-2793.

Weisman, M.L., R. Rotunno, 2004: "A theory for long-lived squall lines" revisited. *J. Atmos. Sci*., **61**, 361-382.

Tables

Table 1: Values of constants and parameters used in the size distribution formulations of MY and MTT throughout all simulations

Parameter	Value	Reference
V-D coefficient for rain	149.1	Tripoli and Cotton (1980)
V-D coefficient for cloud ice	71.34	Ferrier (1994)
V-D coefficient for snow	11.72	Locatelli and Hobbs (1974)
V-D coefficient for graupel	19.3	Ferrier (1994)
V-D coefficient for hail	206.89	Ferrier (1994)
V-D exponent for rain	0.5	Tripoli and Cotton (1980)
V-D exponent for cloud ice	0.6635	Ferrier (1994)
V-D exponent for snow	0.41	Locatelli and Hobbs (1974)
V-D exponent for graupel	0.37	Ferrier (1994)
V-D exponent for hail	0.6384	Ferrier (1994)
m-D coefficient for all hydrometeors	$(\pi/6\rho_x)$	
m-D exponent for all hydrometeors	3	
Bulk density of liquid water	1000 kg m^{-3}	
Bulk density of ice	500 kg m^{-3}	
Bulk density of snow	100 kg m^{-3}	
Bulk density of graupel	400 kg m^{-3}	
Bulk density of hail	900 kg m^{-3}	

.

Table 2: Values N_0 used in the one-moment experiments for all hydrometeor categories.

Category	N_0 value	Reference
Rain	1×10^7	Dudhia (1989)
Snow	2×10^7	Dudhia (1989)
Graupel	4×10^6	Rutledge and Hobbs (1984)
Hail	1×10^5	Milbrandt and Yau (2005)

Table 3: Experiment overview

Experiment name	Description
MTT-BASE	**Baseline two-moment simulation (MTT)**
MTT-2R2S1G	Same as MTT-BASE, except for 1-moment graupel
MTT-2R1S1G	Same as MTT-BASE, except for 1-moment graupel and snow
MTT-1R1S1G	Same as MTT-BASE, except for 1-moment graupel, snow and rain
MTT-H	Same as MTT-BASE, except for rimed ice category set to hail
MTT-GH	Same as MTT-BASE, except for additional ice category for hail
MTT-GH-NT	Same as MTT-GH, except for removed the hail-to-graupel threshold
MTT-WM	Same as MTT-BASE, except for the warm rain and melting formulations and size limiters for all species set to those of MY
MTT-WM-BRK	Same as MTT-WM, except for breakup formulations set back to those of MTT-BASE (breakup threshold 300 μm)
MTT-WM-ICE	Same as MTT-WM, except for ice, snow and graupel deposition and autoconversion set to those of MY
MTT-WM-ICE-COL	Same as MTT-WM-ICE, except for collection formulations set to those of MY
MY-BASE	**Baseline two-moment simulation (MY)**
MY-2R2S1G	Same as MY-BASE, except for 1-moment graupel
MY-2R1S1G	Same as MY-BASE, except for 1-moment graupel and snow
MY-1R1S1G	Same as MY-BASE, except for 1-moment graupel, snow and rain
MY-H	Same as MY-BASE, except for rimed ice category set to hail
MY-GH	Same as MY-BASE, except for additional ice category for hail
MY-GH-NT	Same as MY-GH, except for removed hail-to-graupel threshold

Table 4: Surface precipitation characteristics in all MTT-experiments after 5 hours of simulation. Column headers are, respectively, mean-accumulated surface precipitation across the domain, maximum-accumulated surface precipitation across the domain, precipitation efficiency (PE), and latent heat released within updrafts averaged over the full domain and time (LH, vertical velocity > 0.5 m s^{-1}). Values between brackets denote the difference relative to the baseline simulations (smaller (larger) than 1 indicates lower (higher) values than baseline).

	5 hours			
	Mean (mm)	Max (mm)	PE (%)	LH (10^{-4} K kg^{-1} s^{-1})
MTT-1R1S1G	4.4 (1.01)	84.3 (0.83)	29.4 (0.85)	1.373 (1.15)
MTT-2R1S1G	4.5 (1.03)	88.7 (0.87)	28.2 (0.82)	1.472 (1.23)
MTT-2R2S1G	4.9 (1.12)	98.1 (0.97)	33.7 (0.98)	1.311 (1.10)
MTT-BASE	**4.3**	**101.4**	**34.5**	**1.197**
MTT-H	5.0 (1.16)	142.1 (1.40)	38.3 (1.11)	1.225 (1.02)
MTT-GH	4.0 (0.93)	79.7 (0.79)	24.2 (0.70)	1.614 (1.35)
MTT-GH-NT	4.9 (1.12)	121.1 (1.19)	36.3 (1.05)	1.238 (1.03)
MTT-WM-BRK	5.0 (1.15)	111.2 (1.10)	36.4 (1.06)	1.232 (1.03)
MTT-WM	4.6 (1.06)	181.3 (1.79)	39.0 (1.13)	1.125 (0.94)
MTT-WM-ICE	5.6 (1.28)	204.4 (2.02)	47.0 (1.37)	1.156 (0.97)
MTT-WM-ICE-COL	5.3 (1.22)	187.5 (1.85)	50.5 (1.47)	1.054 (0.88)

Table 5: As in Table 4, but for the MY experiments

	5 hours			
	Mean (mm)	Max (mm)	PE (%)	LH (10^{-4} K kg $^{-1}$ s^{-1})
MY-1R1S1G	5.8 (1.11)	144.5 (0.74)	43.8 (0.88)	1.229 (1.19)
MY-2R1S1G	5.9 (1.12)	170.1 (0.87)	45.0 (0.91)	1.208 (1.17)
MY-2R2S1G	6.0 (1.14)	181.3 (0.93)	44.2 (0.89)	1.271 (1.23)
MY-BASE	**5.3**	**195.6**	**49.5**	**1.033**
MY-H	5.7 (1.08)	179.5 (0.92)	42.5 (0.86)	1.269 (1.23)
MY-GH	5.2 (0.98)	153.8 (0.79)	40.3 (0.81)	1.187 (1.15)
MY-GH-NT	6.2 (1.18)	214.8(1.10)	49.2 (0.99)	1.210 (1.17)

7. Figures

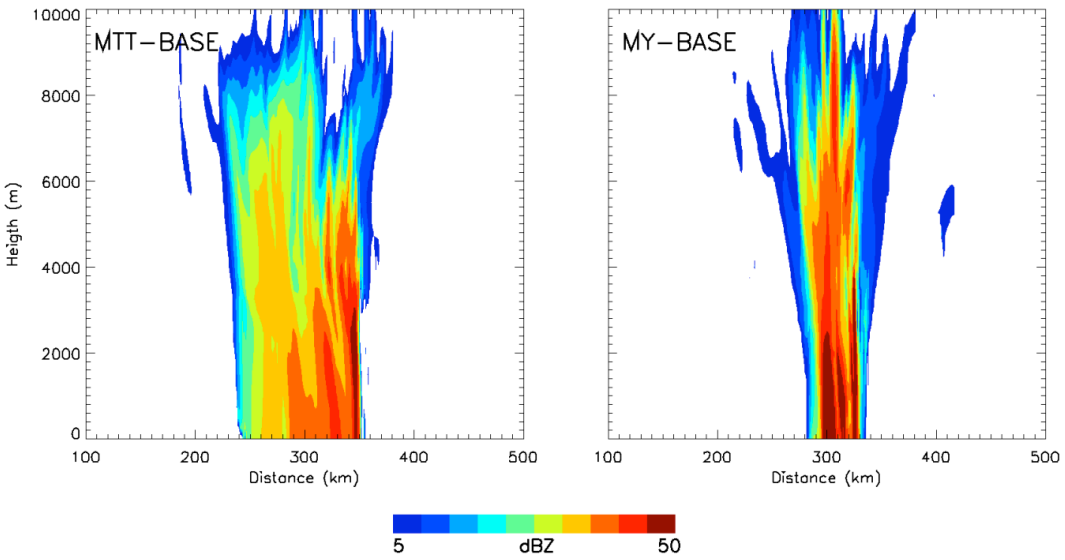

Figure 1: Vertical cross sections of equivalent radar reflectivity for the MTT-BASE (left) and the MY-BASE (right) 4 hours and 30 minutes into the simulation. Total equivalent reflectivity was calculated as the sum of the equivalent reflectivities for each hydrometeor category, as in Milbrandt and Yau (2006).

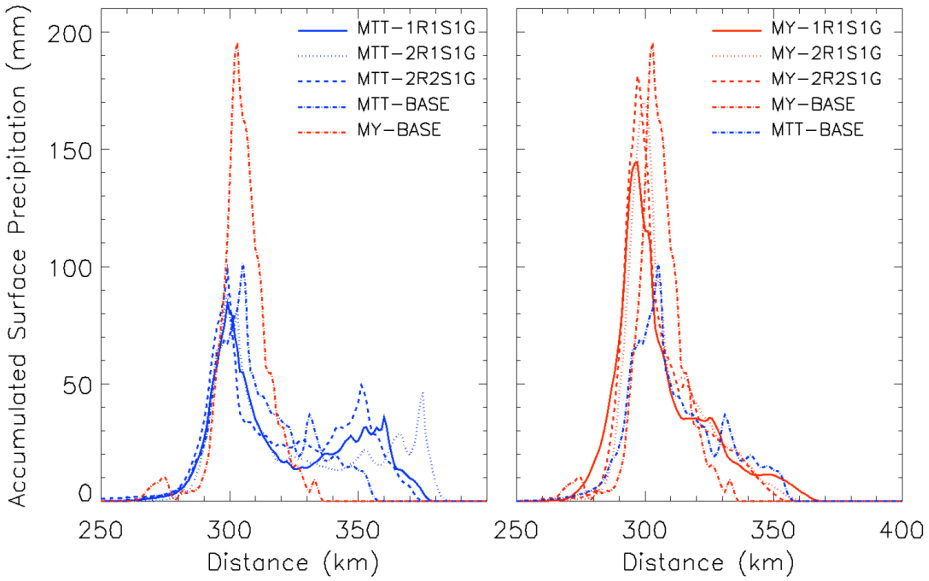

Figure 2: Spatial distribution of accumulated surface precipitation over the full time integration of 5 hours for the experiments on the number of predicted moments for the MTT scheme (left, in blue) and the MY scheme (right, in red). The baseline simulations of the MY (MTT) scheme have been added for reference in the plot depicting the MTT (MY) simulations.

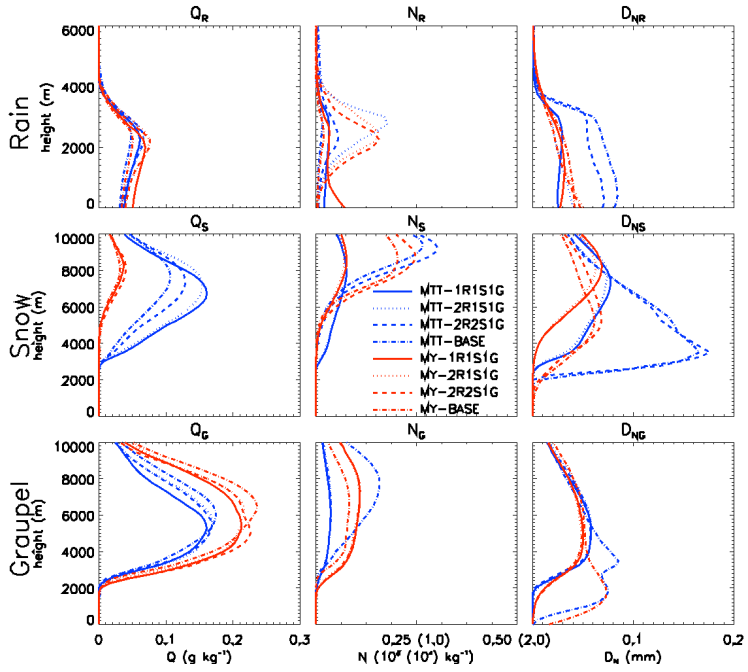

Figure 3: Domain and time averaged vertical profiles of (left) mixing ratio, (center) number concentration and (right) number-weighted mean drop diameter for (top) rain, (middle) snow and (bottom) graupel and for all experiment on the number of predicted moments. MTT experiments are represented in blue and MY experiments in red (solid line: 1R1S1G, dotted line: 2R1S1G, dashed line: 2R2S1G and dash-dotted line: 2R2S2G).

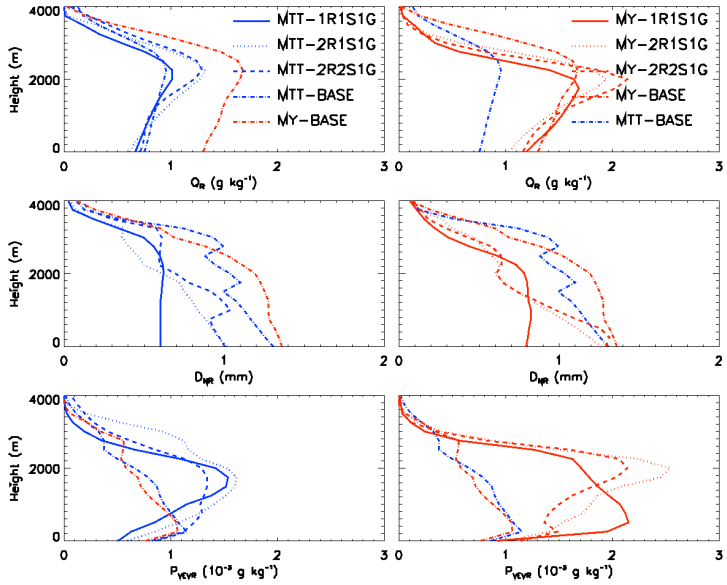

Figure 4: Time-average vertical profiles (top) of mixing ratio, (middle) number-weighted mean drop diameter and (bottom) rain evaporation, associated with the location of maximum surface precipitation accumulation over the full simulation. MTT (left) experiments are represented in blue and MY (right) experiments in red. The baseline simulations of the MY (MTT) scheme have been added for reference in the plot depicting the MTT (MY) simulations.

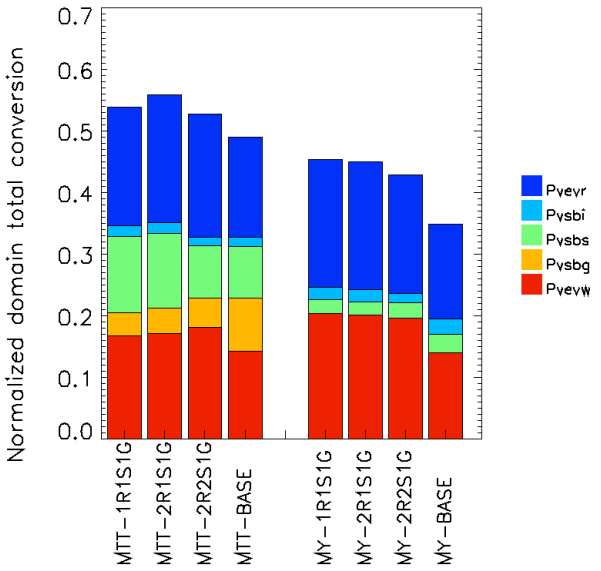

Figure 5: Domain and time integrated total condensate returned to the vapor phase by microphysical processes (given in legend) for each experiment on the number of predicted moments. Values are normalized over the total condensation and deposition for each experiment. Larger normalized total condensate returned to vapor points to lower PE (see appendix 6.2 for explanation of the conversion term acronyms).

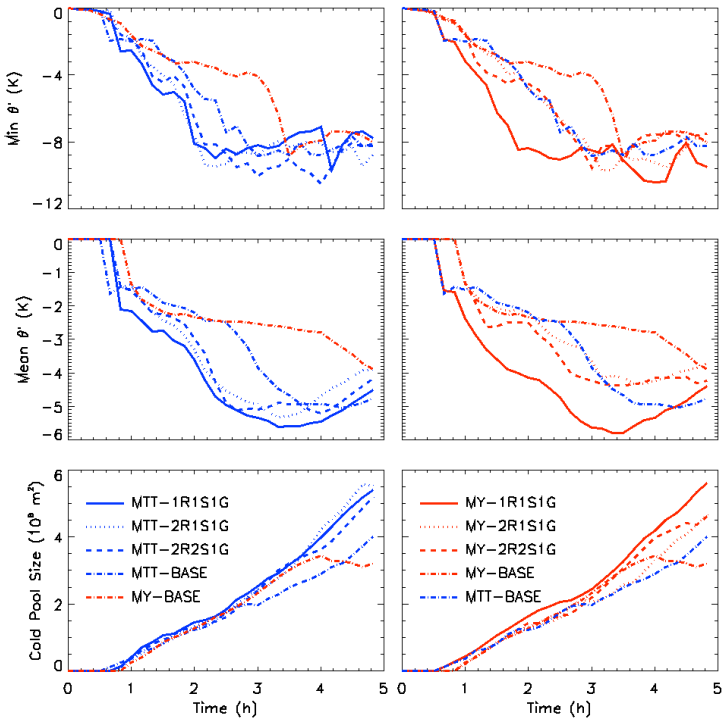

Figure 6: Time evolution of cold-pool characteristics for all experiments on the number of predicted moments for (left) the MTT scheme and (right) the MY scheme (top: maximum cold pool intensity, middle: mean cold pool intensity and bottom: cold pool area). Cold pools are defined by the -1 K isotherm of surface potential temperature perturbation. The baseline simulations of the MY (MTT) scheme have been added for reference in the plot depicting the MTT (MY) simulations.

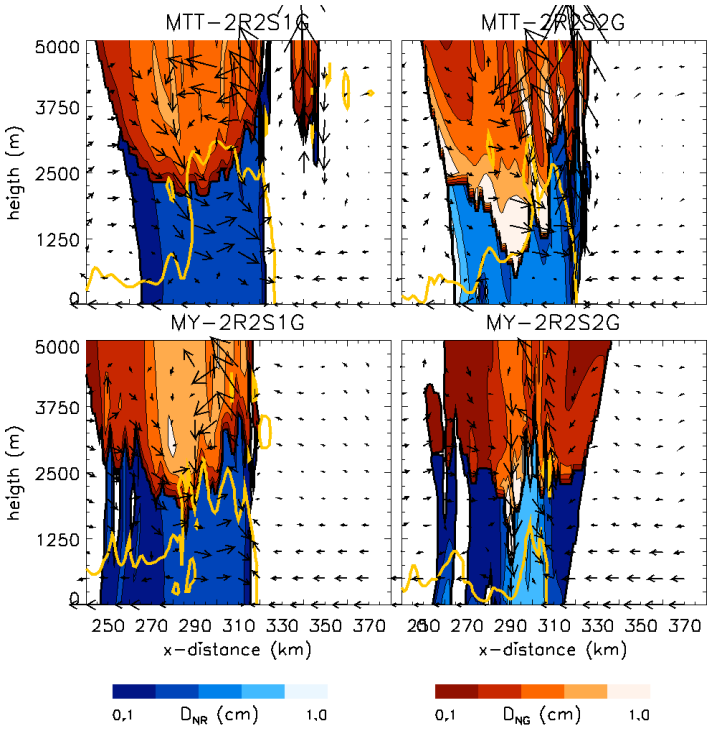

Figure 7a: Vertical cross section through the squall line, 3 hours and 20 minutes into the simulation for the MTT-2R2S1G (upper left), MTT-BASE (upper right), MY-2R2S1G (bottom left) and MY-BASE (bottom right). Shading indicates number-weighted mean particle size for (red) graupel and (blue) rain. Arrows indicate the flow within the squall line, which generally propagates to the right. The yellow solid line indicates the cold pool boundary (-3 K isotherm).

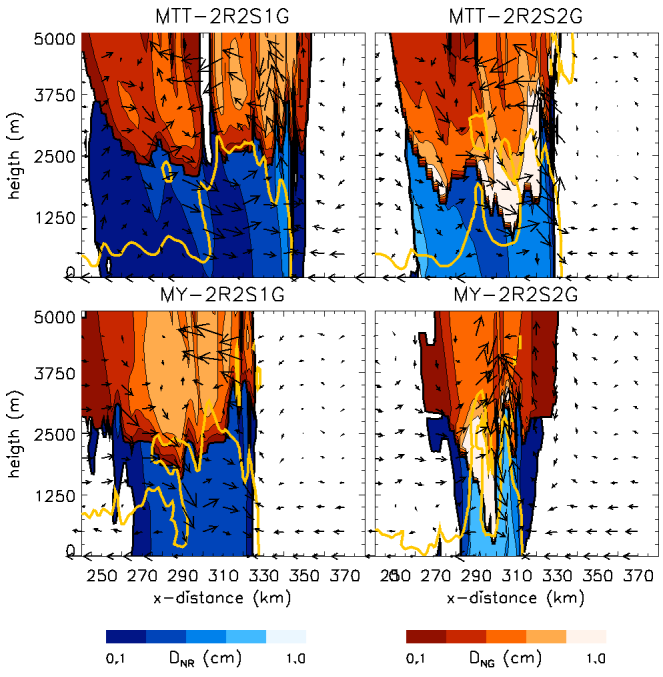

Figure 7b: As Figure 7a, but 3 hours and 50 minutes into the simulation

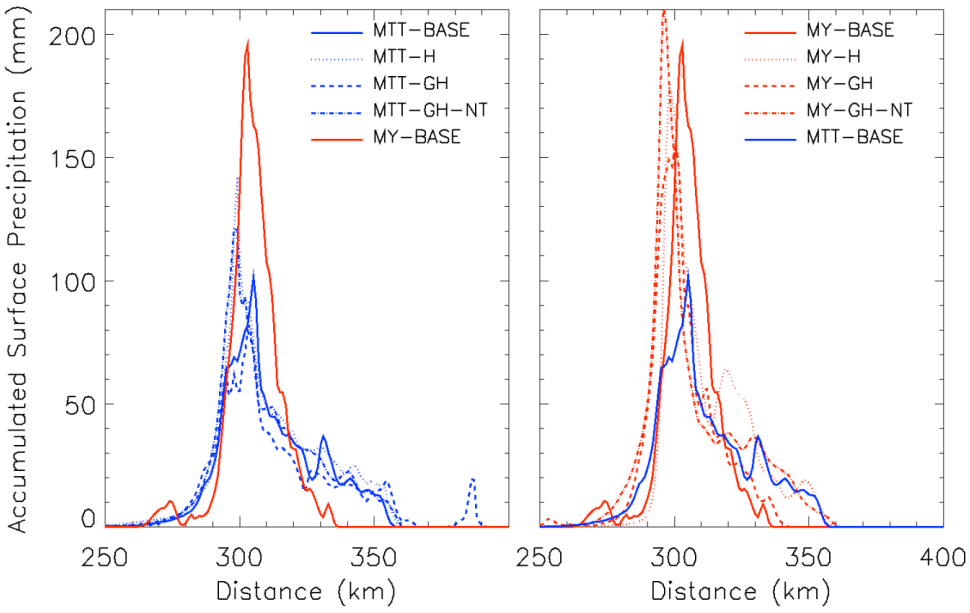

Figure 8: as in Figure 2, but for experiments on the number of ice categories.

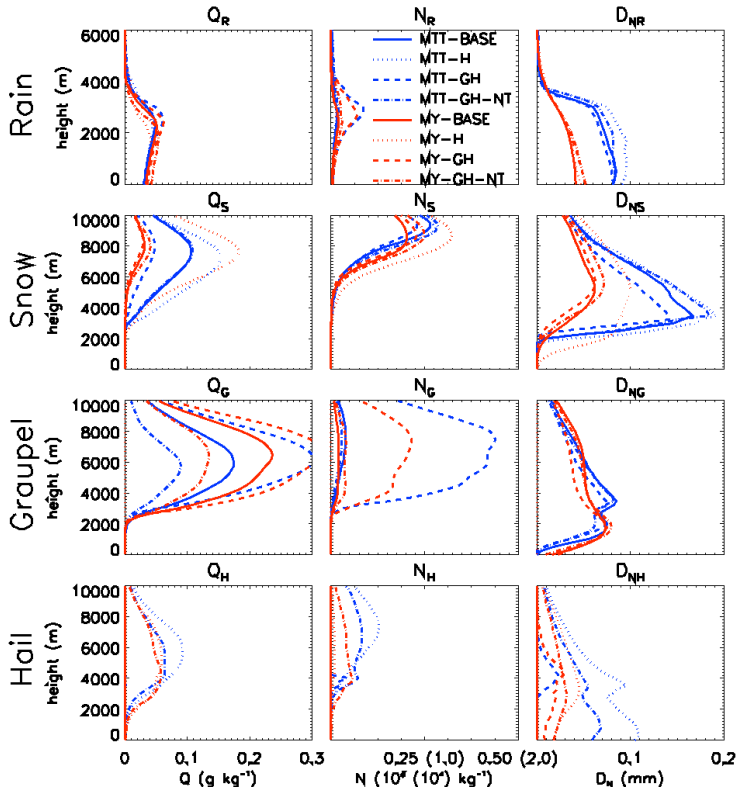

Figure 9: As in Figure 3, but for the experiments on the number of ice categories.

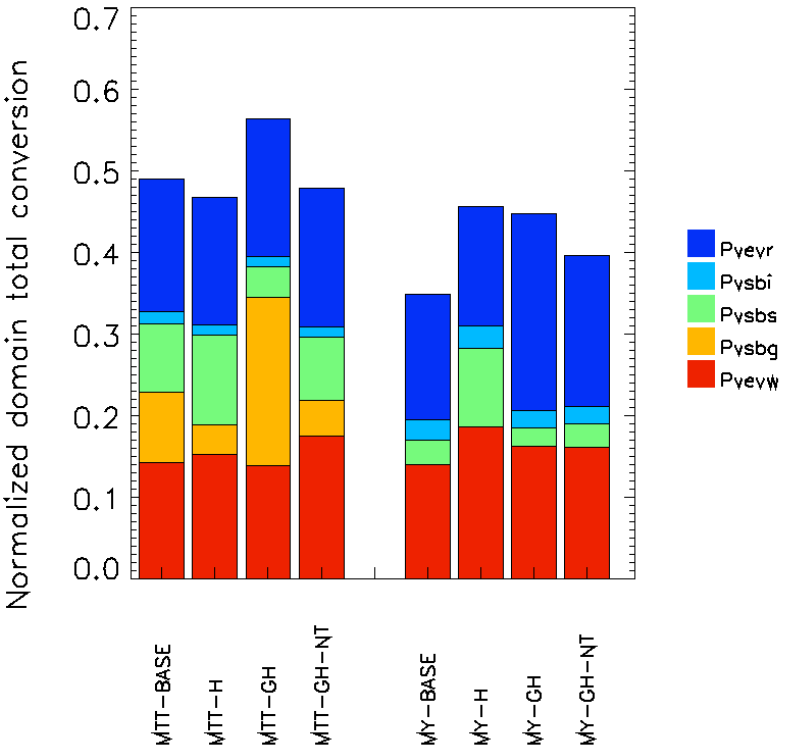

Figure 10: As in Figure 5, but for the experiments on the number of ice categories

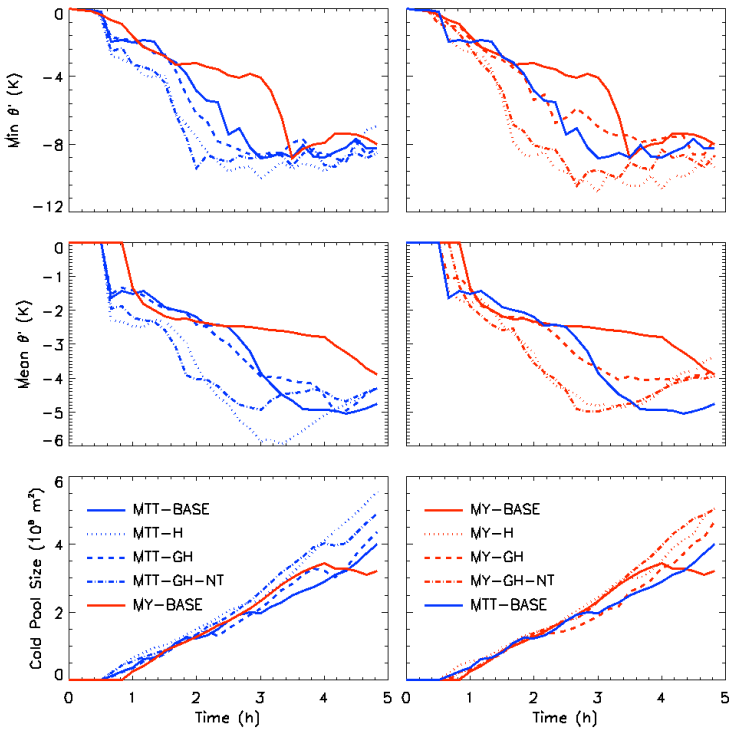

Figure 11: As in Figure 6, but for the experiments on the number of ice categories.

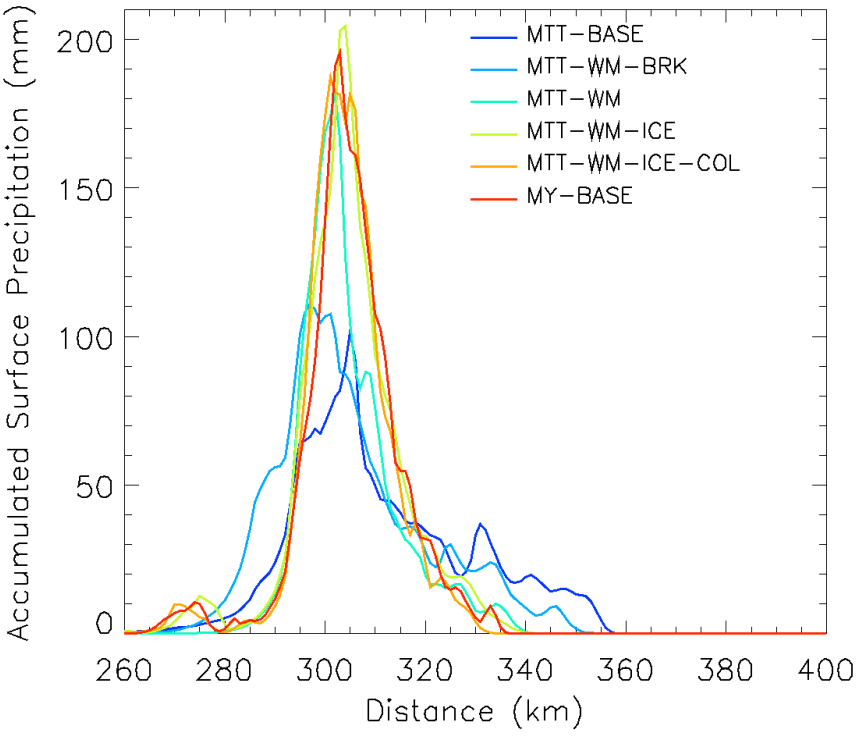

Figure 12: As in Figure 2, but for the experiments on the conversion term formulations

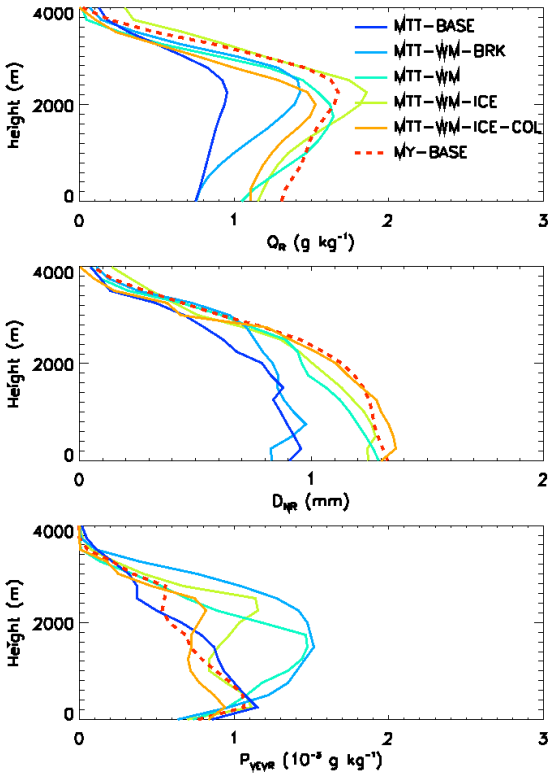

Figure 13: As in Figure 4, but for the experiments on the conversion term formulations

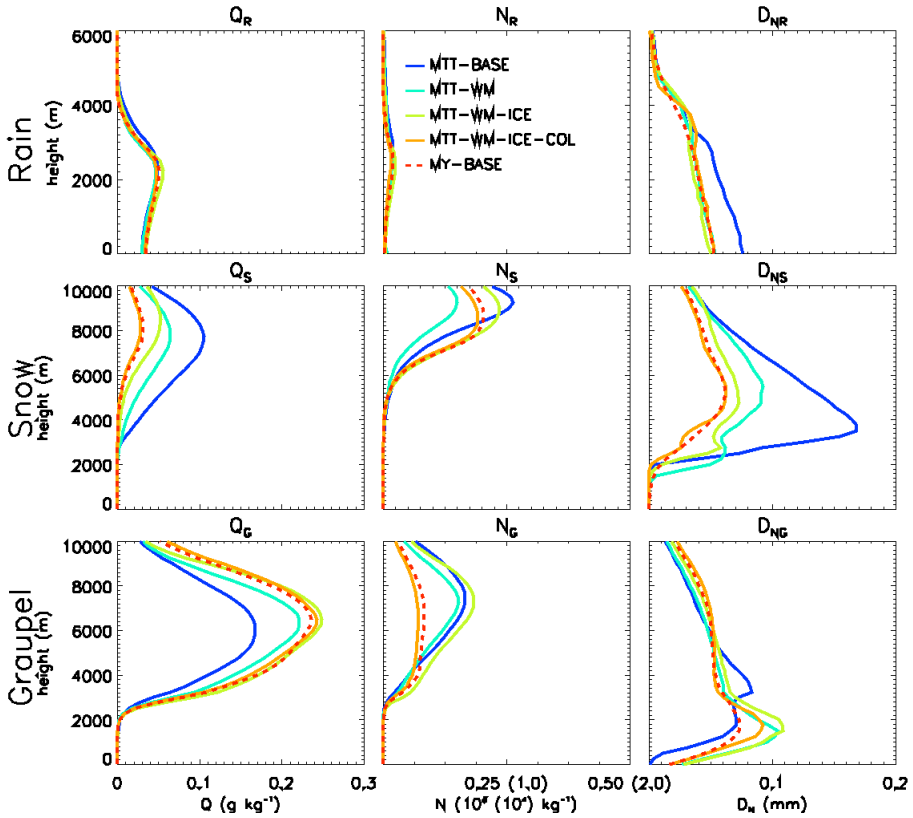

Figure 14: As in Figure 3 but for the experiment on the conversion term formulations

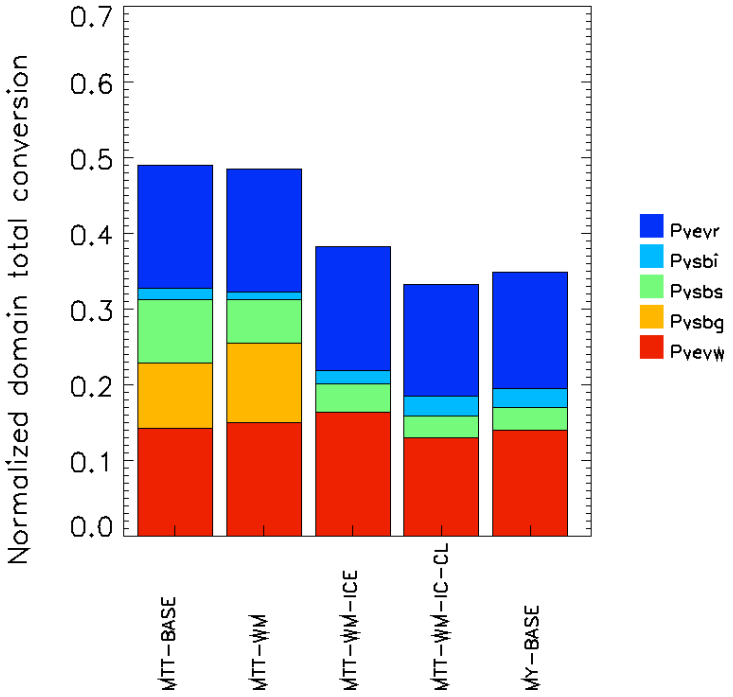

Figure 15: As in Figure 5, but for the experiments on the conversion term formulations

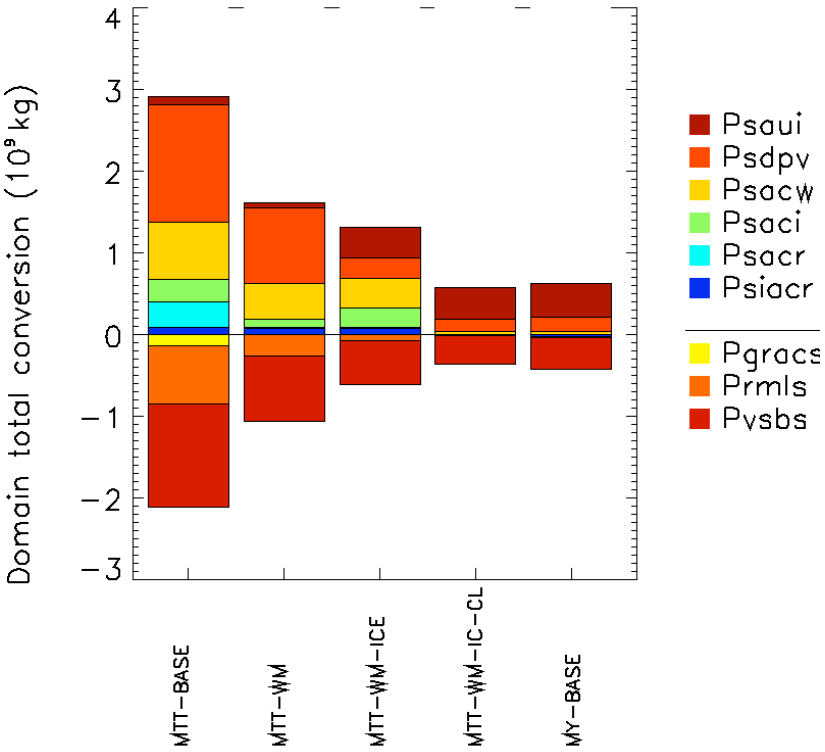

Figure 16: Domain and time integrated total sinks and sources for the snow category associated with microphysical processes (given in legend) for all experiments on the conversion term formulations. A detailed explanation of the abbreviations used for the conversion terms is provided in appendix 6.2.